Solid and aqueous speciation of yttrium in passive remediation systems of acid mine drainage

SCHOLARONE™
Manuscripts

Solid and aqueous speciation of yttrium in

passive remediation systems of acid mine

drainage

Alba Lozano[a,b*], Alejandro Fernández-Martínez[c], Carlos Ayora[a,b], Devis Di Tommaso[d],

Agnieszka Poulain[e], Mauro Rovezzi[f], Carlo Marini[g]

[a] Institute of Environmental Assessment and Water Research, (IDAEA-CSIC), Jordi Girona 18-26, 08034 Barcelona, Spain

[b] Grup de Mineralogia Aplicada i Geoquímica de Fluids, Departament de Cristal·lografia, Mineralogia i Dipòsits Minerals, Facultat de Geologia, Universitat de Barcelona (UB), C/Martí Franquès, S/N, Barcelona, Spain

[c] Univ. Grenoble Alpes, Univ. Savoie Mont Blanc, CNRS, IRD, IFSTTAR, ISTerre, 38000 Grenoble, France

[d] School of Biological Sciences, Queen Mary University of London, Mile End Road, London, E1 4NS, UK

[e] ESRF, The European Synchrotron, 71 Avenue des Martyrs, Grenoble 38000, France

[f] Univ Grenoble Alpes, CNRS, IRD, Irstea, Météo France, OSUG, FAME, 38000 Grenoble, France

[g] CELLS-ALBA Synchrotron Radiation Facility, Carrer de la Llum 2-26,08290 Cerdanyola del Valles, Barcelona, Spain

Corresponding author: Alba Lozano (alba.lozano@idaea.csic.es)

1

21 **ABSTRACT**

22 Yttrium belongs to the rare earth elements (REE) together with lanthanides and

23 scandium. REE are commonly used in modern technologies, and their limited supply

24 has made it necessary to look for new alternative resources. Acid mine drainage (AMD)

25 is a potential resource since is moderately enriched in REE. In fact, in passive

26 remediation systems, which are implemented to minimize the environmental impacts of

27 AMD, REE are mainly retained in basaluminite, an aluminum hydroxysulfate

28 precipitate. In this study, the solid and liquid speciation and the local structure of

29 yttrium were studied in high sulfate aqueous solutions, basaluminite standards and

30 samples from remediation columns using synchrotron-based techniques and molecular

31 modeling. Pair distribution function (PDF) analyses and ab initio molecular dynamics

32 density functional theory models of the yttrium sulfate solution show that the YSO_4^+ ion

33 pair forms a monodentate inner sphere complex. Extended X-ray absorption fine

34 structure (EXAFS) and PDF analyses show that Y is retained by basaluminite forming a

35 monodentate inner-sphere surface complex at the aluminum hydroxide surface. EXAFS

36 of the column samples show that its signal is represented in more than 75% by the

37 signal of a basaluminite which YSO_4^+ is forming an inner-sphere complex. The atomic

38 vision of the REE configuration in AMD environments could help for a deeper research

39 of the REE recovery from waste generated in the AMD remediation systems.

40

2

INTRODUCTION

Yttrium belongs to Rare Earth Elements (REE) group, also composed by lanthanides and scandium. REE are necessary for the development of modern technologies, and specifically, yttrium as important applications, for instance, in fluorescent lamps as phosphors,[1] and in aircraft industry, used in the thermal barrier coatings for jet engines.[2] The REE increasing demand but low worldwide supply has led to consider REE as critical raw materials boosting searches for alternative resources, such as recycling used stocks or identifying new geological sources of these elements. Because the REE concentrations in acid mine drainage (AMD) are from one to two orders of magnitude higher than the average concentrations in natural waters,[3] it may be possible to perform secondary REE recovery from precipitates from AMD neutralization in passive remediation systems. The active systems were developed to minimize the environmental impacts of AMD and they are used worldwide.[4,5] However, due to the high water content, sludge storage has substantial operational costs and environmental concerns.[6,7] In contrast, passive remediation systems, which have been developed extensively in recent decades,[8-11] allow the AMD neutralization generating lower amounts of solid waste precipitates. Ayora et al. documented nearly complete aqueous REE retention in two laboratory columns simulating a disperse alkaline substrate (DAS), a passive treatment already implemented in the field, for two highly acidic AMD (SW Spain).[12,13] The REE were scavenged by basaluminite, a mineral precipitated in the columns, which also presented Y enrichment due to the higher yttrium concentration with respect to the rest of REE in the two treated AMD. Basaluminite, an aluminum oxy-hydroxysulfate $(Al_4(SO_4)(OH)_{10} \cdot 5H_2O)$, precipitates in acidic environments as a consequence of the natural attenuation of the AMD when mixing with more alkaline waters, or due to the induced neutralization of the acid waters, when the solution pH reaches ~4.[14]

3

66   Basaluminite is considered a nanomineral, with a short-range order, around 1 nm of

67   coherent domain size, which is described as layers of Al-octahedra with structural point

68   defects and with the presence of sulfate groups as outer-sphere complexes between the

69   Al layers.[15]

70   Similarly to the REE uptake by basaluminite in DAS treatments, Gammons et al.,

71   reported the precipitation of hydrous aluminum oxides accompanied with a decrease in

72   REE concentration from AMD when mixed with natural water.[16] Recently, the scavenge

73   of REE by basaluminite precipitates has been described as a sorption mechanism.[17]

74   AMD is characterized to contain high loads of dissolved sulfate and the affinity of REE

75   to form aqueous species with sulfate is very high, the MSO_4^+ aqueous complex being

76   the more abundant in AMD solutions.[18] Sorption of dissolved REE from sulfate-rich

77   waters onto basaluminite is thus described as the sorption of the MSO_4^+ aqueous

78   complex via ligand exchange with a surface site of basaluminite, forming a

79   monodentate surface complex with the Al-octahedron as one proton is released.[17] Here,

80   a structural description of the aqueous YSO_4^+ complex and of the local environment of

81   the surface complex formed upon adsorption onto basaluminite are reported.

82   Most of the previous studies reporting the adsorption mechanisms of REE using X-ray

83   absorption spectroscopy and Extended X-ray Absorption Fine Structure (EXAFS)

84   described the adsorption of free REE ions onto the surface of metal oxides.[19-22]

85   However, the AMD environments show a high concentration of dissolved sulfate, which

86   presents high affinity for aqueous REE (M). Thus, the MSO_4^+ aqueous complex is the

87   major REE species in solution and explains that the sorption models of REE in AMD

88   precipitates might be better explained in terms of MSO_4^+ sorption.

89   The structure of the first hydration shell of lanthanides and yttrium has been well

90   characterized.[23-28] The coordination number (CN) of the first hydration shell changes

91   from an average of CN ~ 9 oxygen atoms for light REE (LREE La to Pm) to CN ~ 8

92   oxygen atoms for heavy REE (HREE Tb to Lu), with intermediate values for medium

93   REE (MREE Pm to Gd).[27] This behavior is explained by the continuous decrease in

94   ionic radii with the atomic number.[27,29,30] The ionic radius of yttrium is between that

95   those of Ho and Dy, so it is typically considered an HREE with a first hydration shell of

96   CN ~ 8 oxygen atoms. There are several studies describing aqueous complexes of REE

97   with different ligands. REE easily forms inner-sphere complexes with carbonate and

98   phosphate in solution[31-33] whereas chloride and nitrate forms inner-sphere complexes at

99   concentrations higher than 10 M.[23,25] In the case of sulfate, no information about the

100   geometry of MSO_4^+ complexes has been reported so far despite their strong binding

101   affinity.[18]

102   The objective of this study is to elucidate the structure of Y adsorbed onto basaluminite.

103   Due to its chemical similarities with HREE, this allow us to assume similar structural

104   configuration for this sub-group. Moreover, this element was one of the most

105   concentrated in waste samples allowing performing X-ray absorption spectroscopy

106   experiments. Since the YSO_4^+ aqueous complex is adsorbed onto the mineral,[17] a

107   previous characterization of the geometry of the aqueous complex has been carried out.

108   Finally a quantification of Y-species in basaluminite solids precipitated from AMD

109   treatments has been performed. Structural studies were performed using EXAFS and

110   pair distribution function (PDF) analyses of aqueous and solid samples combined with

111   *ab initio* molecular dynamics (AIMD) simulations of the aqueous YSO_4^+ complexes.

112   Two hypotheses are used to investigate the local structure of the aqueous YSO_4^+ ion

113   pair: (1) an outer-sphere complex, with water located between Y^{3+} and SO_4^{2-}, and (2) an

5

114   inner sphere complex. In the latter case, two more hypotheses must be considered: (a) a

115   monodentate complex, with one oxygen atom shared between the sulfate and the fist

116   coordination sphere of Y^{3+}, and (b) a bidentate complex, with two oxygen atoms shared

117   between the yttrium hydration sphere and the sulfate group.

118   Once the structure of the aqueous solution is fully described, different hypotheses have

119   been considered to interpret the YSO_4^+ surface complexation onto the Al-

120   oxyhydroxysulfate: the formation of (1) a monodentate inner sphere complex, (2) a

121   bidentate mononuclear inner-sphere complex, (3) a bidentate binuclear inner sphere

122   complex.

123   Finally, to determine semi quantitatively the yttrium species in solids from column

124   samples, linear combination fits were performed using the most representative

125   references.

126   **MATERIAL AND METHODS**

127   **Synthetic samples (standards)**

128   Different basaluminites doped with Y were prepared for HEXS and EXAFS

129   experiments. To ensure maximum Y incorporation into the solid, sorption and

130   coprecipitation experiments were performed at pH 6,[17] avoiding higher pH values where

131   YCO_3^+ aqueous species could be present.[34] A basaluminite sample with sorbed YSO_4^+

132   (B-YSO4-ads) was obtained from a suspension of 1g/L of solid in 0.11 $Y(NO_3)_3 \cdot 6H_2O$

133   and 0.25 M Na_2SO_4 solution for 5 hours at a constant pH of 6. At these conditions, the

134   major species in solution was YSO_4^+, which is supposedly the aqueous Y specie sorbed

135   on the solid surface.[17] A basaluminite sample coprecipitated with Y (B-Ycop) was

136   obtained using the basaluminite synthesis method adding 1 M $Y(NO_3)_3 \cdot 6H_2O$ in the

6

137   acid solution of 0.05 M $Al_2(SO_4)_3 \cdot 18H_2O$ (see Chapter S1 of the SI). Basaluminite and

138   nanoboehmite samples with sorbed Y^{3+} (B-Yads and A-Yads, respectively) were also

139   prepared from a suspension of 1 g/L of solid in 0.011-0.11 M $Y(NO_3)_3 \cdot 6H_2O$ solution

140   for 5 hours, and the pH was maintained at ~6 at room temperature, respectively (the

141   synthesis protocol is described in detail in Chapter S1 of the SI). At these conditions,

142   the major species of Y is Y^{3+}. In all cases, the suspensions were centrifuged at 4500 rpm

143   for 15 minutes, the supernatant was filtered through 0.2 μm membranes and kept for

144   ICP analysis. The solids were rinsed several times with deionized water and oven dried

145   for 48 hours at a maximum temperature of 40° C.

146   High-energy X-ray scattering (HEXS) and EXAFS experiments of aqueous solutions

147   with Y and YSO_4^+ were carried out. For the HEXS measurements, an aqueous solution

148   of free yttrium ions (Y-sol) was prepared with 0.1 M $Y(NO_3)_3 \cdot 6H_2O$ at pH 3.2, and a

149   solution containing YSO_4^+ as the major aqueous complex (YSO₄-sol) were prepared by

150   mixing equal amounts of 0.2 M $Y(NO_3)_3 \cdot 6H_2O$ and 0.2 M Na_2SO_4 at pH 3. For the

151   EXAFS measurements, a solution with the free Y^{3+} ion (Y-sol) with a composition of

152   0.01 M $YCl_3 \cdot 6H_2O$ at pH 4.6, and the solution of the YSO_4^+ complex (YSO₄-sol) with a

153   composition of 0.01 M $YCl_3 \cdot 6H_2O$ and 0.01 M Na_2SO_4 at pH 2.9, were prepared,

154   respectively. At these conditions, the major species in solution were Y^{3+} and YSO_4^+

155   (Fig. S1). The yttrium concentrations of the references are listed in Table S1, and a

156   more comprehensive description of the syntheses is given in the Supporting Information

157   S1.

158   Waste samples from column treatments

159   Column samples were collected from two laboratory column experiments of Disperse

160   Alkaline Substrate (DAS), as described in Ayora et al.[12] simulating the remediation

161   systems of the two AMD from the Iberian Pyrite Belt region (SW Spain). The columns

162   (9.6 cm inner diameter and 39 cm in height) consisted in a permeable mixture of grained

163   limestone and wood shavings at a 1:1 weighed ratio. Samples W-MR-C1-4 and W-MR-

164   C1-5 belonged to columns which treated AMD from Monte Romero mine and W-Alm-

165   C3-8 and W-Alm-C3-9 samples belonged to columns which treated leaching of

166   Almagrera mine tailing dam. Y concentration in different AMDs at the inlet ranged

167   from 9 to 42 ppm, and sulfate concentrations 3.5 and 11.7 mg/L. Physical-chemical

168   parameters and water samples were collected every two weeks. Once the treatment

169   finished after 18 weeks, the solid was divided in 2 cm thick slices and dried. The

170   partitioning of Al, Fe and REE was studied by performing a sequential extraction

171   adapted from Torres and Auleda to the solid residues.[35] The results showed in Ayora et

172   al. concluded that REE were retained in basaluminite.[10] The W-MR-C1-4, W-MR-C1-5,

173   W-Alm-C3-8 and W-Alm-C3-9 samples were selected from the depth were maximum

174   Al concentration was extracted from the solids, assuming the most enriched in

175   basaluminite solid slice. These waste samples were used for EXAFS measurements and

176   the Y concentrations for these samples are shown in Table S2.

177   **Analytical techniques**

178   Measurements of the pH values of the initial and final solutions were made with a

179   Crison® glass electrode calibrated with buffer solutions of pH 2, 4 and 7. The Al and S

180   concentrations were measured by inductively coupled plasma optical emission

181   spectroscopy (ICP-OES), and the Y concentration was measured by inductively coupled

182   plasma mass spectrometry (ICP-MS). The aqueous speciation and saturation index of

183   the solid phases were calculated with the PHREEQC code[36] using the Donnee

184   Thermoddem_V1.10 database[37] provided by the Bureau de Recherches Géologiques et

185   Minières (BRGM). Details of the analytical procedures and the database for the REE

186   speciation are described in the Supporting Information S2.

187   The HEXS measurements were performed at the ID31 beamline at the European

188   Synchrotron Radiation Facility (ESRF). The samples were loaded into 1.5 or 2 mm

189   Kapton capillaries, and the HEXS patterns were obtained using a Pilatus3 X CdTe 2M

190   detector. The data correction and generation of structure factors and pair distribution

191   functions were performed with the PDFgetX3 software.[38] PDF for aqueous solutions

192   were obtained by subtracting the scattering signal of pure water from the total scattering

193   signal of YSO4-sol sample and Y-sol sample, respectively. The differential pair

194   distribution functions (d-PDF) for B-Ycop sample were obtained by subtracting the

195   PDF signal of a pure synthetic basaluminite from the PDF of B-Ycop sample.

196   The EXAFS measurements of the samples B-Yads, B-Ycop, A-Yads, Y-sol and YSO4-

197   sol were performed at the Y K-edge (17.038 keV) at the FAME beamline,[39] BM30B at

198   the ESRF. The EXAFS measurements of the B-YSO4 sample was performed at the Y

199   K-edge (17.038 keV) at CLÆSS beamline (ALBA synchrotron). Atomistic models of

200   YSO_4^+ and Y^{3+} complexes adsorbed on a basaluminite surface with different initial

201   configurations were employed in the data analysis to extract the Y local order

202   parameters, including the neighbor distances, R, coordination number, N, and Debye-

203   Waller factors, σ^2. The proportion of Y species present in each waste sample from

204   column treatments was obtained by linear combination fitting (LCF) of the EXAFS

205   spectra using the most representative reference compounds as the basis set. The

206   experimental setup and the details of the data analysis are given in the Supporting

207   Information S3.

208   The Ab Initio Molecular Dynamics (AIMD) simulations of an aqueous solution of

209   yttrium(III) sulfate were carried out on a Y^{3+}–SO_4^{2-}–OH^- system embedded in a box of

210   61 water molecules. The simulations were conducted with the electronic structure code

211   CP2K/Quickstep code, version 5.1.[40] CP2K implements density functional theory

212   (DFT) based on a hybrid Gaussian plane wave. The revPBE generalized gradient

213   approximations for the exchange and correlation terms were used together with the

214   general dispersion correction termed DFT-D3.[41,42] The simulations were carried out for

215   15 ps in the canonical (constant NVT) ensemble to maintain the average temperature at

216   T = 300 K. An in-house Python code using DiffPy-CMI was developed to convert the

217   AIMD trajectories to PDF signals.[43] Details of the MD simulations are described in S4.

218   **RESULTS AND DISCUSSION**

219   **Geometry of the aqueous complex YSO$_4^+$**

220   The experimental (YSO4-sol, Y-sol) and theoretical (YSO4-calc) PDFs of the Y-

221   containing aqueous solutions, 0.1 M YNO$_3$ and YSO$_4$, are shown in Fig. 1. Background

222   subtraction of the aqueous samples was performed using a deionized water background,

223   which implies that the experimental PDFs shown here are differential PDFs (water

224   subtracted). The background scale factor was adjusted to minimize the O-O correlation

225   (~2.8 Å) in the PDFs. All spectra show an intense peak at 2.37 Å, which corresponds to

226   the Y-O interatomic distances to oxygen in the first coordination shell. The

227   experimental PDF of the YSO4-sol sample shows a small and sharp peak at 1.45 Å that

228   corresponds unequivocally to the S-O interatomic distance in sulfate, and another

229   smaller peak at ~3.6 Å, which is absent in Y-sol sample. The DFT-based PDFs obtained

230   from AIMD simulations of the YSO_4^+ aqueous complex also reproduced this latter

231   peak. Analyses of the AIMD trajectories show that the 3.6 Å distance between Y and S

232   is consistent with the formation of a monodentate inner sphere complex (one shared

233   oxygen) between the coordination shells of the sulfur and yttrium.
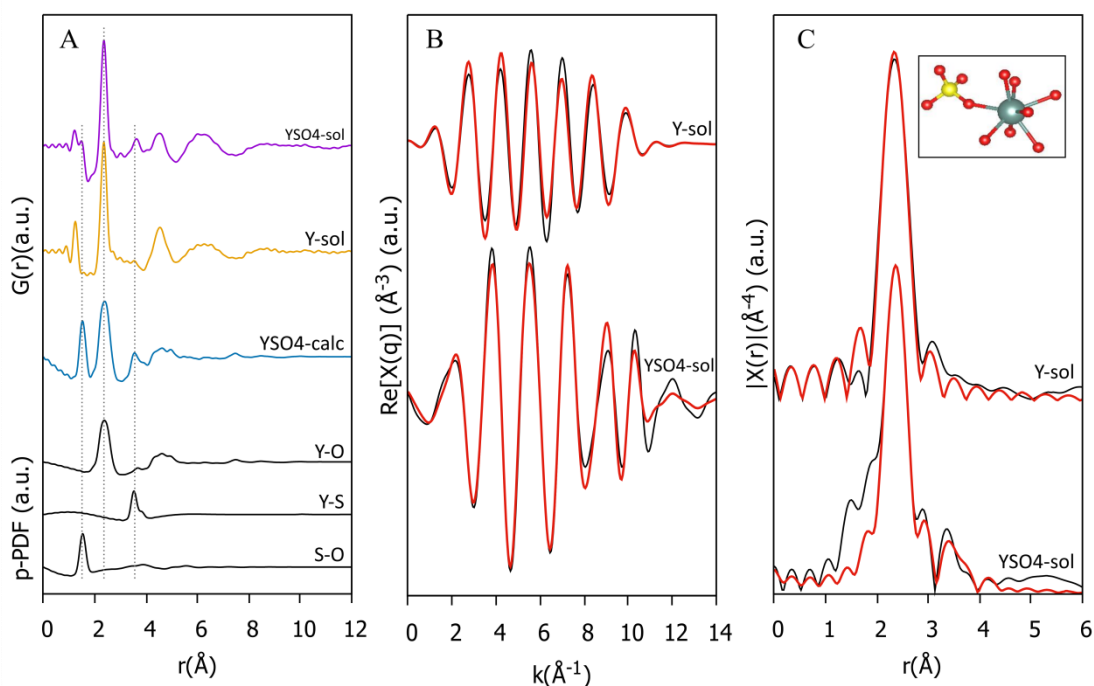
235   Figure 1. (A) Top: Experimental PDFs of YSO4-sol and Y-sol samples. Bottom:

236   Simulated (AIMD) PDF (YSO4-calc) and partial PDFs of an YSO_4^+ aqueous complex.

237   (B) Fourier-filtered signal from 1.8 to 4.2 Å for the EXAFS data. (C) EXAFS FT

238   amplitude functions of the YSO4-sol sample. Black lines: experimental; red lines: fits.

239   Simulated (AIMD) PDF and partial PDFs have been multiplied for visualization

240   purposes: YSO_4-cal (×3), Y-S (×5) and Y-O and S-O (×2). Dashed lines indicate the

241   position of the Y-O, Y-S and S-O bonds in YSO4-sol sample.

242   Fits of the EXAFS spectra of the aqueous solutions were performed using atomistic

243   models from the AIMD simulations as initial structural models for the generation of the

244   scattering paths. The results yielded an average Y-O distance of 2.37 ± 0.02 Å for the

245   Y-sol sample and 2.38 ± 0.01 Å for YSO4-sol (Table 1). The intense peak in the FT

246   function at 2.38 Å for the two aqueous references represents the first solvation shell,

247   and its asymmetry reveals a distribution of Y-O interatomic distances, as reported

248   previously by Lindqvist et al.[24] The coordination numbers (CN) were 7.6 ± 1.9 and $7.9 \pm$

249   0.9 for Y-sol and YSO4-sol, respectively, which are close to the expected value of 8 for

250   HREE. A second shell is visible in the FT of the YSO4-sol sample. It was fitted with a

251   Y-S distance of 3.50 ± 0.04 Å, similar to that observed in the PDF of the same sample,

252   and a CN = 1. This corresponds to a monodentate coordination, matching the geometry

253   obtained from the AIMD simulations. The coordination number CN = 1 was kept fixed

254   in the EXAFS fitting to increase the stability of the fitting procedure, minimizing the

255   number of parameters and excessive correlations between them. A multiple scattering

256   path (Y-S-O) was included and was found to be relevant and to improve the fit. The

257   fitting parameters matched both the PDF and modeling results and indicated that the

258   YSO_4^+ aqueous species forms a monodentate inner-sphere complex.

259   Table 1. Modeling parameters of the Y K-edge EXAFS spectra of the 0.1 M YSO_4

260   aqueous solution (the error is expressed in the parentheses after the last digit).

Sample	Neighbor	path	N	σ^2	ΔE_0	R (Å)	Var.	χ_v^2
Y sol	1st shell	Y-O	7(2)	0.005(3)	-2(3)	2.37(2)	4	354
Y-SO4 sol	1st shell	Y-O$_1$	7.9(9)	0.007(2)		2.38(1)	8	498
	2nd shell	Y-S	1 $_{fixed}$	0.003(6)	-1(1)	3.50(4)		
	3rd shell	Y-S-O	1 $_{fixed}$	0.015(19)		3.18(10)		

12

261   The determined Y-O first shell coordination numbers and interatomic distances are

262   consistent with previous reports describing yttrium coordination shells with N = 8 and

263   Y-O distances of 2.36 Å.[23,24,28] Likewise aqueous REE carbonate and phosphate

264   complexes,[31-33] aqueous Y-SO4 ion-pairs form inner-sphere complexes. This result

265   contrasts with other ligands such as chloride, which hardly forms inner sphere

266   complexes at similar concentrations to those used in this study.[23] Only the formation of

267   monodentate complexation between Dy and NO_3 with a distance of 3.57 Å has been

268   reported using MD simulations.[26]

Local order of yttrium adsorbed into basaluminite

270   HEXS measurements were performed on a pure basaluminite sample (B-pure) and on a

271   sample of basaluminite coprecipitated with Y (B-Ycop). The PDFs are shown in Fig. 2

272   with the differential PDF obtained by subtracting the pure sample from the

273   coprecipitated one. This approach has been previously used to examine the local order

274   of different anions incorporated in poorly crystalline minerals, such as schwertmannite

275   and basaluminite, and the desorption of sulfate from basaluminite when ageing at

276   circumneutral pH values.[15,46] The PDFs of the two samples are similar and show

277   characteristic basaluminite peaks that correspond to the known interatomic distances (S-

278   O bond at ~1.46 Å, Al-O bonds at 1.88, 4, 4.8 and 6 Å and Al-Al bonds at 3 Å).[15,45] The

279   differential PDF shows a main peak at 2.37 Å, which corresponds to the Y-O distance.

280   This peak matches the distance from Y to the first solvation shell obtained from the

281   EXAFS and PDF of the Y^{3+} and YSO_4^+ aqueous solutions (Fig. 1). Another peak is

282   present at 1.7 Å, which is tentatively assigned to a new Al-O distance of the Al-

283   octahedra, due to probable distortions of the basaluminite. The existence of

284   deformations in the structures of mineral nanoparticles upon oxyanion adsorption has

285   been previously observed.[44,46] A smaller peak appears at 3.48 Å, which can be

13

286   tentatively assigned to a Y-S distance, though it is shorter than the Y-S distance

287   reported for the YSO_4^+ aqueous complex (Table 2 and Fig. 1A). This peak may also

288   correspond to a Y-Al interatomic distance, which would be consistent with the

289   formation of an inner-sphere complex, as suggested by Lozano et al.[17] This hypothesis

290   will be tested using different atomistic models for the fitting of the EXAFS data. Other

291   peaks at longer distances are difficult to assign in the absence of a more detailed

292   structural model.
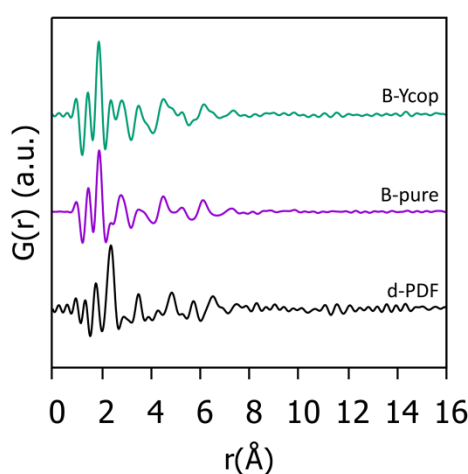
293

294   Figure 2. PDFs of basaluminite coprecipitated in the presence of Y (B-Ycop), pure

295   basaluminite (B-pure) and differential PDF (d-PDF). The d-PDF spectrum has been

296   amplified (×3) for visualization purposes.

297   The k^3-weighted EXAFS spectra for the solid references B-YSO4-ads, B-Y-ads, B-Y-

298   cop and A-Y-ads (Fig. 3) are indistinguishable and differ from the aqueous Y-sol and

299   YSO4-sol spectra in that a slight oscillation becomes visible at 5-6 $Å^{-1}$. In the B-YSO4-

300   ads the dominant Y species in solution is the YSO_4^+ complex. However, in B-Y-ads, B-

301   Ycop and A-Yads, the dominant Y species is Y^{3+}. Still, these four samples show similar

302   spectra. Since the common feature in these three samples is the presence of an Al

303   adsorbent, and this feature agrees with that in the B-YSO4-ads EXAFS spectrum, we

14

304   hypothesize that the higher frequency observed at 5-6 Å^{-1} (arrow in Fig. 3) may be

305   related to the presence of an Al backscatterer, rather than to a signal from an close

306   sulfate group. Both Al and S are light atoms with similar atomic numbers (Z = 13 and

307   16, respectively), which makes their backscattering functions difficult to distinguish via

308   fitting of the EXAFS signal. These observations lead us to assume that the EXAFS

309   measurements have poor sensitivity to the presence of Y-S bonds in this system.

310   However, a contribution from a sulfate shell for the two first samples cannot be ruled

311   out.
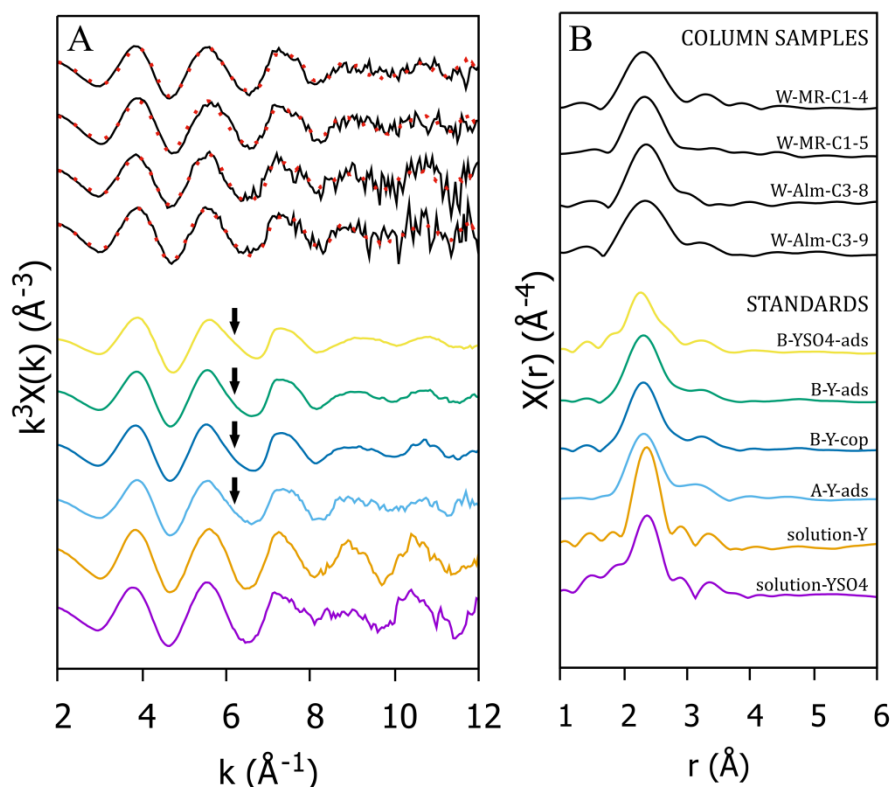
312   [A1]

313   Figure 3. k^3-weighted EXAFS (A) and FT amplitude functions (B) for four waste

314   samples from column treatments W-MR-C1-3, W-MR-C1-4, W-Alm-C3-8, and W-

315   Alm-C3-9 (upper part) and solid standards (basaluminite sorbed with YSO4. (B-YSO4),

316   basaluminite sorbed and coprecipitated with Y: B-Yads and B-Ycop, respectively) and

317   aqueous solution (free ion and sulfate complex: Y-sol and YSO4-sol, respectively)

318   (bottom part). The dashed lines in the EXAFS signals of the column samples represent

319   LCF with B-Yads (basaluminite with sorbed yttrium) and YSO4-sol (solution of Y with

320   SO_4) standards as the most representative references (results in Table 3). The arrows

321   indicate a frequency present in the solid standards.

322   Based on the previous information of the aqueous species and on the thermodynamic

323   model of REE sorption,[17] the B-YSO4-ads EXAFS signal was fitted with three models

324   of different geometries of the YSO_4^+ aqueous complex adsorbed onto basaluminite

325   surfaces via inner-sphere complexes (Fig. 4), to obtain an atomistic model

326   representation: (A) a monodentate surface complex; (B) a bidentate mononuclear

327   surface complex and (C) a bidentate binuclear surface complex.
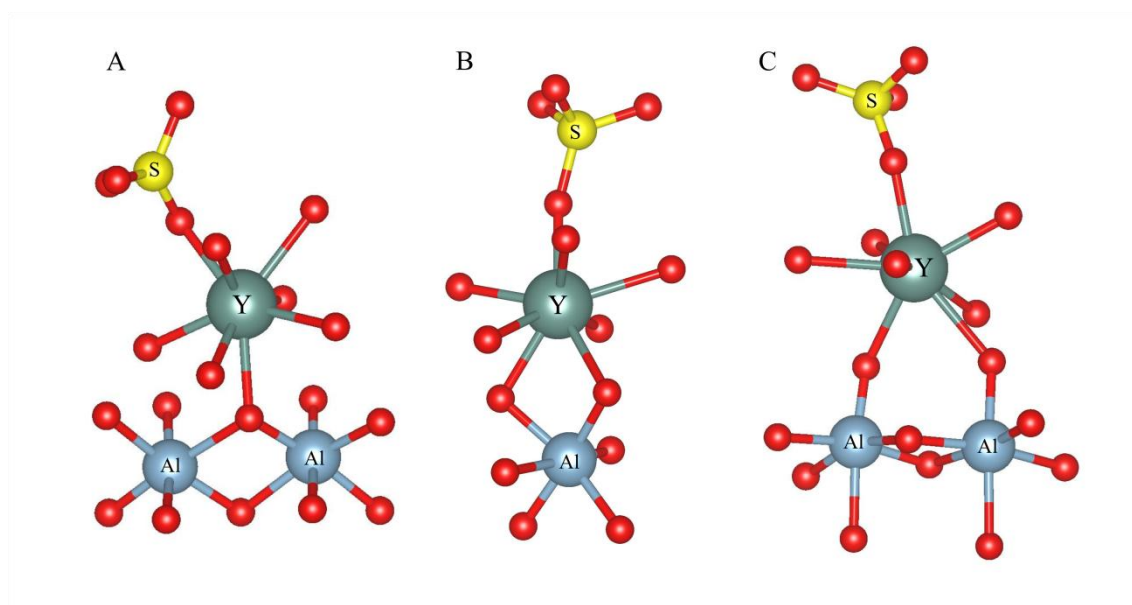
328

329   Figure 4. Atomistic representations of the three models of YSO4 aqueous complex

330   adsorbed on the basaluminite-water interface. The different atomic positions of YSO4

331   to octahedral-Al are used to fit the EXAFS signal of the B-YSO4 sample. The three

16

332   models show different inner-sphere surface complexes: (A) monodentate, (B) bidentate

333   mononuclear and (C) bidentate binuclear.

334   The EXAFS fits for B-YSO4-ads for the different models and the calculated parameters

335   are given in Fig. 5 and Table 2, respectively. The first model represents a monodentate

336   inner-sphere surface complex. The coordination number of the shells has been fixed

337   based on information from another sources: The major aqueous species in solution was

338   YSO_4^+, which, as supported by PDF and DFT data, forms a monodentate aqueous

339   complex. Besides, the thermodynamic model of REE sorption on basaluminite indicated

340   monodentate complexation of the YSO_4^+ aqueous complex.[17] With this information the

341   fit was performed assuming S and Al coordination numbers equal to 1 and 2,

342   respectively, as it is shown in Fig. 4A. Besides, two oxygen paths were considered due

343   to the Y-O length variation improving the fit. Thus, the fit yielded a first coordination

344   shell with a Y-O distance range between 2.32 and 2.47 ± 0.02 Å with a fix coordination

345   number of 8. The second shell was fitted yielding a Y-Al distance at 3.52 Å with a fixed

346   coordination number of N = 2, and a Y-S distance at 3.33 with a fixed number of N = 1.

347   This result is consistent with the monodentate inner-sphere complex of Y with one

348   oxygen shared with two surface Al sites (Fig. 4A). The second model, the bidentate

349   binuclear inner-sphere complex configuration, gave poorer results without structural

350   significance and with higher χ_v^2 values (Table 2), so it was discarded. The third model

351   was the bidentate binuclear, the first shell was fitted with a coordination number of 10 ±

352   1.31 and a distance of 2.33 Å. The second shell was fitted with a S path yielding an Y-S

353   distance of 3.34 Å with a fix coordination number of N = 1, similar to that for the

354   monodentate hypothesis, and with an Al path with a fixed coordination number of N = 2

355   giving a distance a bit longer, 3.92 Å.

356   Overall, the monodentate inner-sphere surface complex gave the best fit results, which

357   was in accordance to the thermodynamic sorption model. Moreover, the bidentate

358   binuclear inner-sphere surface complexes yielded also a good fit with similar χ_v^2 values

359   than the monodentate hypothesis, making this configuration also possible (Fig. 4C). In

360   both fits, the distances between Y-S are similar, 3.33, 3.34 Å, which is also observed in

361   the differential PDF of the B-Ycop reference. From the EXAFS data, the presence of a

362   bidentate binuclear surface complex cannot be ruled out. However, the thermodynamic

363   modeling and the EXAFS data both agree on the monodentate surface complex being

364   the one present at the basaluminite-water interface.
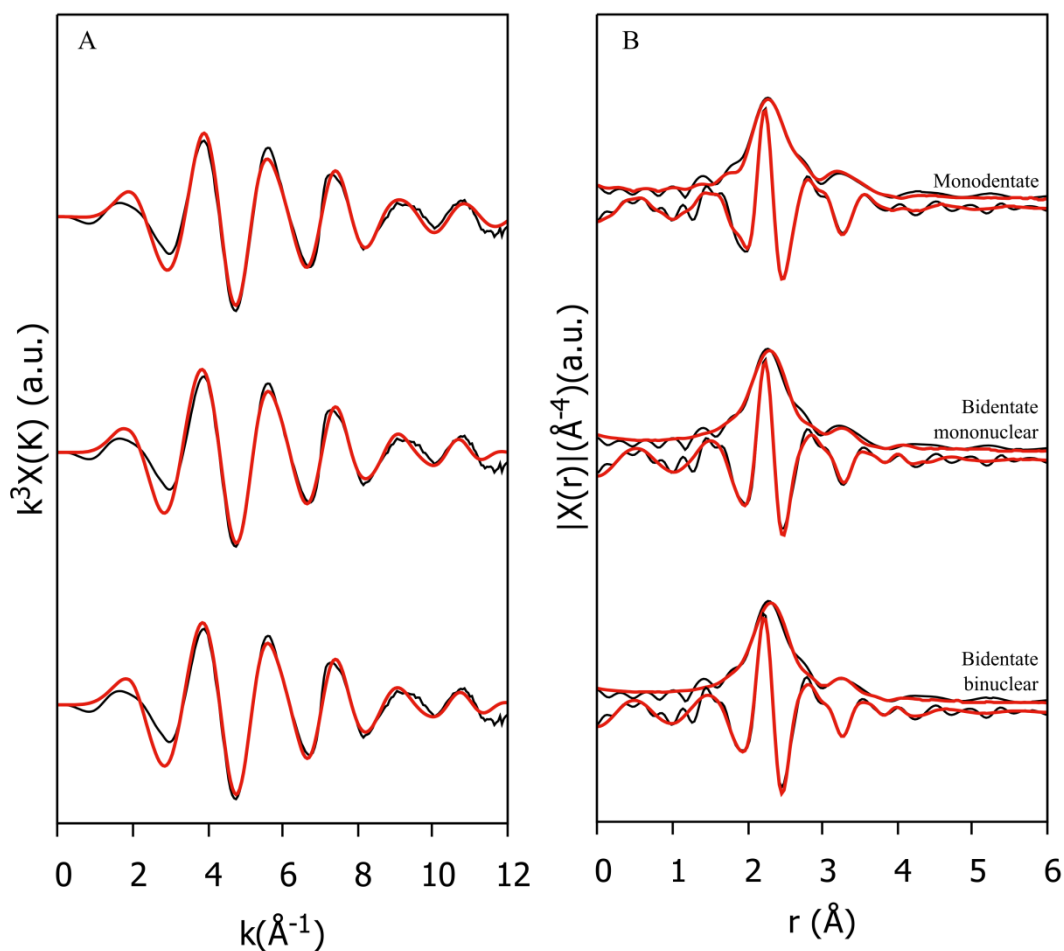
365

366   Figure 5. (A) The k^3-weighted EXAFS spectra at the Y K-edge of the basaluminite with

367   YSO4 sorbed (B-YSO4 reference) and (B) its Fourier transform amplitude. The

368   experimental and fitted curves are shown in black and red, respectively.

369   Table 2. Results of the EXAFS fits for B-YSO4 reference. Model 1: monodentate inner

370   sphere. Model 2: bidentate mononuclear inner sphere. Model 3: bidentate binuclear

371   inner sphere. Var. indicates independent variables. The best model is indicated with a

372   star (*). The error is expressed in the parentheses after the last digit.

Model	Neighbor	path	N	σ^2	ΔE_0	R	Var.	χ_v^2
1*	1st shell	Y-O$_1$	6$_{fix}$	0.007(1)	-3(2)	2.32(1)	9	338
		Y-O$_2$	2$_{fix}$	0.004(8)	-3(2)	2.47(2)		
	2nd shell	Y-S	1$_{fix}$	0.008(5)	-3(2)	3.33(4)		
		Y-Al	2$_{fix}$	0.012(5)	-3(2)	3.52(5)		
2	1st shell	Y-O	10 (1)	0.012(2)	-6(2)	2.33 (1)	8	402
	2nd shell	Y-S	1$_{fix}$	0.009(5)	-6(2)	3.88 (5)		
		Y-Al	1$_{fix}$	0.006(3)	-6(2)	3.42 (3)		
3	1st shell	Y-O	10(1)	0.013(1)	-4(1)	2.33(1)	8	334
	2nd shell	Y-S	1$_{fix}$	0.008(3)	-4(1)	3.34(3)		
		Y-Al	2$_{fix}$	0.011(5)	-4(1)	3.92(4)		

373

374   The EXAFS of the B-YSO4-ads standard was also fitted with the same three atomistic

375   models presented in Fig. 4 but without sulfate included (Fig. S2) to analyze the

376   sensitivity of the fit to the presence of sulfate. The Al-O distances obtained with these

377   new fits (Table S3) were almost identical to those calculated when including sulfate

378   shells (Table 2), with the exception in the monodentate inner sphere configuration,

379   which was a bit longer. Thus, the presence of Al is consistent in the two models, with

380   and without sulfate. However, the fits obtained with the sulfate group included showed

381   lower values of the agreement factor (reduced chi-square) (compare Table 2 and Table

382   S3). This discussion highlights the difficulties of the EXAFS technique to discern the

383   presence of low-Z backscatterers, in particular in disordered systems such as the one

384   present here.

385   These results are consistent with those presented by Rabung et al. where Gd and Lu

386   were shown to adsorb onto γ-Al_2O_3 to form inner sphere complexes.[47] Lu, which is

387   considered a HREE such as Y, was shown to form a monodentate surface complex with

388   a first shell of 7 atoms and a Lu-O distance of 2.28 Å. The longer Y-O distance found

389   here for Y is consistent with its larger Y ionic radius. However, these authors could not

390   detect any Lu-Al bonds in their EXAFS data. Other sorption studies of Eu onto γ-Al_2O_3

391   showed the formation of both monodentate and bidentate binuclear complexes.[20] In

392   contrast to this study and to the results of Rabung et al. on Al oxides, EXAFS studies of

393   lanthanides sorbed onto ferric oxides have shown a predominance of bidentate inner-

394   sphere complexes.[47] Lu adsorbed onto ferrihydrite at pH ≥ 5.5 yielded an Lu-O

395   coordination number of 7 at a distance of 2.30 Å, and a second coordination shell was

396   identified with a Lu-Fe interatomic distance at 3.38 Å. These EXAFS results were

397   complemented by time-resolved laser fluorescence spectroscopy (TRLF) measurements

398   that showed five water molecules surrounding the metal cations, which was interpreted

399   as a bidentate inner sphere complex.[22] The similar distance to the second shell found by

400   Dardenne et al.[22] and by us in these two different systems can be explained by the

401   smaller size of Lu in comparison to Y, which is compensated for by the longer Fe-O

402   bond distance in comparison to the Al-O bond, making possible a bidentate

403   mononuclear sphere at 3.4 Å in Fe oxides and Al oxides. Another study by Estes et al.

404   reported Eu K-edge EXAFS data of Eu(III) sorbed onto hematite.[19] They observed a

405   decrease in the coordination number of the Eu-O bond from 8 to 5 upon adsorption

406   accompanied by a smaller Eu-Fe bond distance at 3 Å. This result was interpreted via

407   molecular simulations as being due to the formation of an inner sphere bidentate

20

408   mononuclear surface complex. Such a decrease in the coordination number was not

409   observed in this study; the CN of the Y-O correlation was maintained at ~8 ± 1 for both

410   the aqueous and surface complexes.

411   **Identification of Y species in waste samples from AMD treatment**

412   The k^3-weighted EXAFS of the column samples (upper part) and standards (lower part)

413   and their Fourier transform (FT) envelope functions with corrected phase-shifts are

414   shown in Fig. 3. Visual comparisons of the EXAFS spectra of the column samples

415   reveal a strong similarity between them, suggesting similar local order of Y in all

416   samples. In addition, the EXAFS spectra of the column samples are very similar to solid

417   references (B-YSO4-ads, B-Y-ads, B-Y-cop and A-Y-ads). They have a shoulder at

418   ~6.5 $Å^{-1}$, indicating a higher frequency which is absent in the aqueous samples (see

419   arrow in Fig. 3).

420   Based on the PCA analyses (see Chapter S3), the reconstructed spectra indicated that

421   only two components were required to describe the samples (Fig. S4). The two most

422   likely Y species identified by target transformation of the standard spectra, were the B-

423   YSO4-ads and B-Y-ads references (Fig. S5). However, since their EXAFS signals are

424   very similar, LCF of the EXAFS spectra of the waste samples from column treatments

425   was performed using B-YSO4-ads and YSO4-sol (Fig. 3A, upper part) to quantify the

426   proportions of different Y species in the waste samples. The use of these two standards

427   would correspond to YSO_4^+ adsorbed forming inner- and outer-sphere complexes,

428   respectively.

429   The LCF results show that more than 75% of Y adopts a local geometry similar to that

430   of the B-YSO4-ads reference (with the exception of sample W-Alm-C3-8, for which the

431   LCF indicated equal proportion of both YSO4 presented as inner sphere and outer-

432 sphere complexes (Table 3)). The waste samples were selected from the depth where the

433 major proportion of Al precipitated, assuming basaluminite precipitation. However,

434 other minor mineral species may have also been precipitated, such as Fe-

435 oxyhydroxisulfate, due to the presence of small amount of Fe in the solids. Specifically,

436 samples from Almagrera column (W-Alm-C3-8 and W-Alm-C3-9) presented higher Fe

437 concentration than samples from Monte Romero treatment. REE can be also scavenged

438 by amorphous Fe hydroxides in AMD neutralization environments,[48] so a minor or

439 almost negligible fraction of Y could be retained by the small proportion of ferric

440 oxides precipitated in the selected samples, explaining the lower proportion of B-YSO4-

441 ads.

442 Table 3. Percentages of Y species in the column samples obtained from LCF of the

443 EXAFS spectra. R-factor and χ^2 are defined in Chapter S3 of the SI.

Standard	C1-4	C1-5	C3-8	C3-9
B-YSO4ads	0.719 ± 0.036	0.867 ± 0.038	0.495 ± 0.059	0.746 ± 0.061
YSO4-solution	0.281 ± 0.069	0.133 ± 0.071	0.505 ± 0.084	0.254 ± 0.085
R-factor	0.14	0.14	0.29	0.30
χ^2	133	154	371	392

444

445 **ENVIRONMENTAL IMPLICATIONS**

446 The YSO_4^+ aqueous species has been characterized combining PDF analyses of aqueous

447 solutions and AIMD simulations, confirming the formation of an inner-sphere Y-SO_4

22

448   ion pair with a monodentate configuration, with an Y-S interatomic distance of 3.5 Å.

449   Results from thermodynamic sorption model describe REE sorption onto basaluminite

450   via sorption of aqueous $REESO_4^+$. The use of an atomistic model using this positively

451   charged ion yields the best results for the EXAFS fitting of Y sorbed on basaluminite.

452   However, the EXAFS technique cannot confirm the presence of YSO_4^+ sorbed into

453   basaluminite by itself, due to the low sensitivity to discern between Al and S neighbors.

454   Rather than this, the EXAFS fitting, together with the PDF, can confirm the strong

455   interaction and the formation of inner-sphere surface complexes of Y onto basaluminite

456   precipitates, via ligand exchange with AlO_6 units of its structure. EXAFS analyses of

457   column waste samples show that most of the Y is retained as the same inner-sphere

458   sorbed species, YSO_4^+, with a low proportion of YSO4+ in outer-sphere configuration.

459   The description of the local structure of yttrium sorbed onto the basaluminite surface

460   provided here complements the atomic configuration studies of other trace metals, such

461   as As and Se oxyanions.[44] The chemical similarity between yttrium and other HREE

462   (from Tb to Lu) suggests that similar environments could be present for the other

463   elements of the same group. This fact has important environmental consequences, as the

464   HREE would be strongly sorbed, via covalent bonds, which could result in their long-

465   term immobilization at least until the host phase is dissolved or re-precipitated. A key

466   question emerges about the long-term stability of the complex, particularly with an

467   increase in the solution pH. The structural evolution of pure basaluminite with

468   increasing pH showed its recrystallization onto boehmite, releasing sulfate into the

469   solution.[45] Previous studies on poorly crystalline Fe phases from AMD such as

470   schwertmannite have shown a release of adsorbed toxic elements during aging due to

471   recrystallization processes.[49] The occurrence of such processes in REE-doped

472   basaluminite could result in the remobilization of REEs and of other potentially

23

473   adsorbed toxic elements. The extent to which these processes can occur in natural

474   waters requires further investigation.

475   Further studies on the potential uptake of LREEs by basaluminite are necessary to

476   confirm and/or compare different structural mechanisms to those of their HREE

477   counterpart, as an step to develop separation methods for REEs. These investigations

478   will help to enhance a selective recovery of REE from AMD wastes and thus to

479   generate an economic value of the waste generated during the neutralization of AMD-

480   affected waters.

481   **Associated information**

482   Supporting information. The supporting information contains 1) five chapters with

483   detailed description of synthesis of reference materials, analytical procedures and

484   aqueous speciation calculations, synchrotron experiments and data analyses, molecular

485   dynamics simulations and the Phyton code used to generate PDF from AIMD

486   simulations; 2) three 3 tables describing samples used for EXAFS measurements and

487   the modeling parameters from EXAFS fitting; and 3) four figures illustrating fitting of

488   EXAFS spectra.

489   **Acknowledgements**

References

501   **References**

502   (1) Binnemans, K.; Jones, P. T.; Blanpain, B.; Van Gerven, T.;, Yang, Y.; Walton, A.;

503   Buchert, M. Recycling of rare earths: A critical review. *J. Clean. Prod.* **2013**, *51*, 1–22.

504   https://doi.org/10.1016/j.jclepro.2012.12.037

505   (2) Kumar, R.; Jiang, C.; Wang, J.; Cietek, D.; Roth, J.; Gell, M.; Jordan, E. H. (2018).

506   Low Thermal Conductivity Yttrium Aluminum Garnet Thermal Barrier Coatings Made

507   by the Solution Precursor Plasma Spray: Part II—Planar Pore Formation and CMAS

508   Resistance.   *J.   Therm.   Spray   Techn.*   **2018**,   27(5),   794–808.

509   https://doi.org/10.1007/s11666-018-0727-x

510   (3) Noack, C. W.; Dzombak, D. A.; Karamalidis, A. K. Rare Earth Element

511   Distributions and Trends in Natural Waters with a Focus on Groundwater. *Environ. Sci.*

512   *Technol.* **2014**, *48* (8), 4317–4326. https://doi.org/10.1021/es4053895.

513   (4) Evangelou V. P.; Zhang, Y. L. A Review: Pyrite Oxidation Mechanisms and Acid

514   Mine Drainage Prevention. *Crit. Rev. Environ. Sci. Technol.* **1995**, *25* (2), 141–199.

515   https://doi.org/10.1080/10643389509388477.

516   (5) Coulton, R.; Bullen, C.; and Hallet, C. The design optimisation of active mine water

517   treatment plants. *Land Contam.Reclamat.* **2003,** *11*, 273-280.

518   (6) Ackman, T. Sludge disposal from acid mine drainage treatment. U.S. Bureau of

519   Mines, *Report of Invest.* 8672, **1982**. Pittsburg, PA. 38 pp.

520   (7) Viadero, R. C.; Wei, X.; Buzby, K. M. Characterization and Dewatering Evaluation

521   of Acid Mine Drainage Sludge from Ammonia Neutralization. *Environ. Eng. Sci.* **2006**,

522   *23* (4), 734–743. https://doi.org/10.1089/ees.2006.23.734.

26

523   (8) Hedin, R. S.; Watzlaf, G. R.; Nairn, R. W. Passive Treatment of Acid Mine

524   Drainage with Limestone. *J. Environ. Qual.* **1994**, *23* (6), 1338–1345.

525   https://doi.org/10.2134/jeq1994.00472425002300060030x.

526   (9) Younger, P. L.; Banwart, S. A.; Hedin, R. S. *Mine Water Hydrology, Pollution,*

527   *Remediation* 2002. https://doi.org/10.1007/978-94-010-0610-1.

528   (10) Cravotta, C. A. Size and performance of anoxic limestone drains to neutralize

529   acidic mine drainage. *J. Environ. Qual.* **2003**, *32*, 1277− 1289.

530   (11) Watzlaf, G. R.; Schroeder, K. T.; Kleinmann, R. L. P.; Kairies, C. L.; Nairn, R. W.

531   The Passive Treatment of Coal Mine Drainage; laboratory report DOE/NETL-

532   2004/1202; U.S. Department of Energy, National Energy Technology Laboratory:

533   Pittsburgh, PA, 2004.

534   (12) Ayora, C.; Macías, F.; Torres, E.; Lozano, A.; Carrero, S.; Nieto, J.-M.; Pérez-

535   López, R.; Fernández-Martínez, A.; Castillo-Michel, H. Recovery of Rare Earth

536   Elements and Yttrium from Passive-Remediation Systems of Acid Mine Drainage.

537   *Environ.   Sci.   Technol.*   **2016**,   *50*   (15)   8255–8262.

538   https://doi.org/10.1021/acs.est.6b02084.

539   (13) Ayora, C.; Caraballo, M. A.; Macias, F.; Rötting, T. S.; Carrera, J.; Nieto, J. M.

540   Acid Mine Drainage in the Iberian Pyrite Belt: 2. Lessons Learned from Recent Passive

541   Remediation Experiences. *Environ. Sci. Pollut. Res.* **2013**, *20* (11), 7837−7853.

542   https://doi.org/10.1007/s11356-013-1479-2

543   (14) Bigham, J. M.; Nordstrom, D K. Iron and aluminum hydroxysulfate minerals from

544   acid sulfate waters. **2000** In: Jambor, J.L., Alpers, C.N., Nordstrom, D.K. (Eds.), Sulfate

545   Minerals, Crystallography, Geochemistry and Environmental Significance, vol. *40*.

546   *Mineralogical Society of America Reviews in Mineralogy and Geochemistry,* pp. 351–

547   403.

548   (15) Carrero, S.; Fernandez-Martinez, A.; Pérez-López, R.; Lee, D.; Aquilanti, G.;

549   Poulain, A.; Lozano, A.; Nieto, J.-M. The Nanocrystalline Structure of Basaluminite, an

550   Aluminum Hydroxide Sulfate from Acid Mine Drainage. *Am. Mineral.* **2017**, *102* (12),

551   2381–2389. https://doi.org/10.2138/am-2017-6059.

552   (16) Gammons, C. H.; Wood, S. A.; Pedrozo, F.; Varekamp, J. C.; Nelson, B. J.; Shope,

553   C. L.; Baffico, G. Hydrogeochemistry and Rare Earth Element Behavior in a

554   Volcanically Acidified Watershed in Patagonia, Argentina. *Chem. Geol.* **2005**, *222* (3–

555   4), 249–267. https://doi.org/10.1016/j.chemgeo.2005.06.002.

556   (17) Lozano, A.; Ayora, C.; Fernández-Martínez, A. Sorption of rare earth elements

557   onto basaluminite: the role of sulfate and pH. *Geochim. Cosmochim. Acta* **2019**. *258*,

558   50-62.

559   (18) Gimeno Serrano, M. J.; Auqué Sanz, L. F.; Nordstrom, D. K. REE Speciation in

560   Low-Temperature Acidic Waters and the Competitive Effects of Aluminum. *Chem.*

561   *Geol.* **2000**, *165*, 167–180. https://doi.org/10.1016/S0009-2541(99)00166-7(19) Estes,

562   S. L.; Arai, Y.; Becker, U.; Fernando, S.; Yuan, K.; Ewing, R. C.; Zhang, J.; Shibata, T.;

563   Powell, B. A. A Self-Consistent Model Describing the Thermodynamics of Eu(III)

564   Adsorption onto Hematite. *Geochim. Cosmochim. Acta* **2013**, *122*, 430–447.

565   https://doi.org/10.1016/j.gca.2013.08.023.

566   (20) Yang, S.; Sheng, G.; Montavon, G.; Guo, Z.; Tan, X.; Grambow, B; Wang, X.

567   Investigation of Eu(III) immobilization on γ-Al_2O_3 surfaces by combining batch

568   technique and EXAFS analyses: Role of contact time and humic acid. *Geochim.*

569   *Cosmochim. Acta* **2013**, *121*, 84-104.

570   (21) Fan, Q. H.; Tan, X. L.; Li, J. X.; Wang, X. K.; Wu, W. S.; Montavon, G. Sorption

571   of Eu(III) on Attapulgite Studied by Batch, XPS, and EXAFS Techniques. *Environ. Sci.*

572   *Technol.* **2009**, *43* (15), 5776–5782. https://doi.org/10.1021/es901241f..

573   (22) Dardenne, B. K.; Schäfer, T.; Denecke, M. A.; Rothe, J.; Kim, J. I. Identification

574   and Characterization of Sorbed Lutetium Species on 2-Line Ferrihydrite by Sorption

575   Data Modeling , TRLFS and EXAFS. *Radiochim. Acta* **2001**, *89*, 469–479.

576   (23) Allen, P. G.; Bucher, J. J.; Shuh, D. K.; Edelstein, N. M.; Craig, I. Coordination

577   Chemistry of Trivalent Lanthanide and Actinide Ions in Dilute and Concentrated

578   Chloride Solutions FT Magnitude. *Inorg. Chem.* **2000**, *39* (11), 595–601.

579   (24) Lindqvist-Reis, P.; Lambe, K.; Pattanaik, S.; Persson, I.; Sandström, M. Hydration

580   of the Yttrium (III) Ion in Aqueous Solution . An X-Ray Diffraction and XAFS

581   Structural   Study.   *J.   Phys.   Chem.   B*   **2000**,   *104*,   402–408.

582   https://doi.org/10.1021/jp992101t.

583   (25) Yaita, T.; Narita, H.; Suzuki, S.; Tachimori, S.; Motohashi, H.; Shiwaku, H.

584   Structural Study of Lanthanides(III) in Aqueous Nitrate and Chloride Solutions by

585   EXAFS.   *J.   Radioanal.   Nucl.   Chem.*   **1999**,   *239*   (2),   371–375.

586   https://doi.org/10.1007/BF02349514.

587   (26) Duvail, M.; Ruas, A.; Venault, L.; Moisy, P.; Guilbaud, P. Molecular Dynamics

588   Studies of Concentrated Binary Aqueous Solutions of Lanthanide Salts: Structures and

589   Exchange   Dynamics.   *Inorg.   Chem.*   **2010**,   *49*   (2),   519–530.

590   https://doi.org/10.1021/ic9017085.

591 (27) Kowall, T.; Foglia, F.; Helm, L.; Merbach, A. E. Molecular Dynamics Simulation

592 Study of Lanthanide Ions Ln^{3+} in Aqueous Solution Including Water Polarization.

593 Change in Coordination Number from 9 to 8 along the Series. *J. Am. Chem. Soc.* **1995**,

594 *117* (13), 3790–3799. https://doi.org/10.1021/ja00118a015.

595 (28) Ohta, A.; Kagi, H.; Tsuno, H.; Nomura, M.; Kawabe, I. Influence of Multi-Electron

596 Excitation on EXAFS Spectroscopy of Trivalent Rare-Earth Ions and Elucidation of

597 Change in Hydration Number through the Series. *Am. Mineral.* **2008**, *93* (8–9), 1384–

598 1392. https://doi.org/10.2138/am.2008.2628.

599 (29) Rizkalla, E. N., Choppin, G. R. Lanthanides and Actinides Hydration and

600 Hydrolysis. In: Handbook on the Physics and Chemistry of Rare Earths. **1994**.

601 (Gschneider, K. A., Eyring, L., Choppin, G. R., Lander, G. H., eds.) Vol. 18 –

602 Lanthanides/Actinides: Chemistry. Elsevier Science B.V., Amsterdam, The

603 Netherlands.

604 (30) Duvail, M.; Spezia, R.; Vitorge, P. A Dynamic Model to Explain Hydration

605 Behaviour along the Lanthanide Series. *Chemphyschem* **2008**, *9*, 693–696.

606 https://doi.org/10.1002/cphc.200700803.

607 (31) Janicki, R.; Starynowicz, P.; Mondry, A. Lanthanide carbonates. *Eur. J. Inorg.*

608 *Chem.* **2011**, 24, 3601–3616. https://doi.org/10.1002/ejic.201100184.

609 (32) Jeanvoine, Y.; Miró, P.; Martelli, F.; Cramer, C. J.; Spezia, R. Electronic structure

610 and bonding of lanthanoid(III) carbonates. Phys. Chem. Chem. Phys. **2012**, 14 (43),

611 14822–14831. https://doi.org/10.1039/c2cp41996c.

612 (33) Harris, S. M.; Nguyen, J. T.; Pailloux, S. L.; Mansergh, J. P.; Dresel, M. J.;

613 Swanholm, T. B.; Gao, T.; Pierre, V. C. Gadolinium complex for the catch and release

614   of phosphate from water. Environ. Sci. Technol. **2017**, 51 (8), 4549–4558.

615   https://doi.org/10.1021/acs.est.6b05815.

616   (34) Luo, Y. R.; Byrne, R. H. Carbonate complexation of yttrium and the rare earth

617   elements in natural rivers. *Geochim. Cosmochim. Acta* **2004**, 68, 691–699.

618   (35) Torres, E.; Auleda, M. A Sequential Extraction Procedure for Sediments Affected

619   by Acid Mine Drainage. *J. Geochemical Explor.* **2013**, *128*, 35–41.

620   (36) Parkhurst, D. L.; Appelo, C. A. J. User´s guide to PhreeqC (version 2.18) A

621   computer program for speciation, and inverse geochemical calculations, U.S.

622   Department of the Interior, U.S. Geological Survey **1999**.

623   (37) Blanc, P.; Lassin, A.; Piantone, P.; Azaroual, M.; Jacquemet, N.; Fabbri, A.;

624   Gaucher, E. C. Thermoddem: A Geochemical Database Focused on Low Temperature

625   Water/Rock Interactions and Waste Materials. *Appl. Geochemistry* **2012**, *27* (10), 2107–

626   2116. https://doi.org/10.1016/j.apgeochem.2012.06.002.

627   (38) Juhás, P.; Davis, T.; Farrow, C. L.; Billinge, S. J. L. PDFgetX3: a rapid and highly

628   automatable program for processing powder diffraction data into total scattering pair

629   distribution   functions.   *J.   Appl.   Crystallogr.*   **2013**,   *46*,   560–566.

630   https://doi.org/10.1107/S0021889813005190.

631   (39) Proux, O.; Biquard, X.; Lahera, E.; Menthonnex, J. J.; Prat, A.; Ulrich, O.; Soldo,

632   Y.; Trévisson, P.; Kapoujyan, G.; Perroux, G.; Taunier, P.; Grand, D.; Jeantet, P.;

633   Deleglise, M; Roux, J-P. and Hazemann, J-L. FAME A New Beamline for XRay

634   Absorption Investigations of Very Diluted Systems of Environmental, Material and

635   Biological   Interests.   *Phys.   Scr.*   **2005**,   970-973.

636   https://doi.org/10.1238/physica.topical.115a00970.

637   (40) Hutter, Y.; Iannuzzi, M.; Schiffmann, F.; VandeVondele, J. CP2K: Atomistic

638   Simulations of Condensed Matter Systems. *Wiley Interdiscip. Rev. Comput. Mol. Sci.*

639   **2014**, *4*, 15–25.

640   (41) Zhang, Y.; Yang, W. Comment on 'Generalized Gradient Approximation Made

641   Simple". *Phys. Rev. Lett*. **1998,** *80,* 890–890.

642   (42) Grimme, S.; Antony, J.; Ehrlich, S.; Krieg, H. A Consistent and Accurate Ab Initio

643   Parametrization of Density Functional Dispersion Correction (DFT-D) for the 94

644   Elements   H-Pu.   *J.   Chem.   Phys.*   **2010**,   *132*   (15),   154104.

645   https://doi.org/10.1063/1.3382344.

646   (43) Juhás, P.; Farrow, C. L.; Yang, X.; Knox, K. R.; Billinge, S. J. L. Complex

647   Modeling : A Strategy and Software Program for Combining Multiple Information

648   Sources to Solve Ill Posed Structure and Nanostructure Inverse Problems. *Acta*

649   *Crystallogr.   Sect.   A   Found.   Adv.*   **2015**,   *A71*,   562–568.

650   https://doi.org/10.1107/S2053273315014473.

651   (44) Carrero, S.; Fernandez-Martinez, A.; Pérez-López, R.; Poulain, A.; Salas-Colera,

652   E.; Nieto, J. M. Arsenate and Selenate Scavenging by Basaluminite: Insights into the

653   Reactivity of Aluminum Phases in Acid Mine Drainage. *Environ. Sci. Technol.* **2017**, *51*

654   (1), 28–37. https://doi.org/10.1021/acs.est.6b03315.

655   (45) Lozano, A.; Fernández-Martínez, A.; Ayora, C.; Poulain, A. Local Structure and

656   Ageing of Basaluminite at Different pH Values and Sulphate Concentrations. *Chem.*

657   *Geol.* **2018**, *496*, 25–33. https://doi.org/10.1016/j.chemgeo.2018.08.002.

658   (46) Cruz-Hernández, P.; Carrero, S.; Pérez-López, R.; Fernández-Martínez, A.;

659   Lindsay, M. B .J.; Dejoie, C.; Nieto, J. M. Influence of As(V) on precipitation and

660   transformation of schwertmannite in acid mine drainage-impacted waters. *Eur. J.*

661   *Mineral.* **2018** https://doi.org/10.1127/ejm/2019/0031-2821.

662   (47) Rabung, Th.; Geckeis, H.; Wang, X. K.; Rothe, J.; Denecke, M. A.; Klenze, R.;

663   Fanghäel, Th. Cm(III) sorption onto γ-Al_2O_3: New insight into sorption mechanisms by

664   time-resolved laser fluorescence spectroscopy and extended X-ray absorption fine

665   structure. *Radiochim. Acta* **2006**, *94*, 609-618.

666   (48) Verplanck, P. L.; Nordstrom, D. K.; Taylor, H. E.; Kimball, B. A. Rare earth

667   element partitioning between hydrous ferric oxides and acid mine water during iron

668   oxidation. *Appl. Geochem.* **2004**, *19*, 1339–1354.

669   (49) Acero, P.; Ayora, C.; Torrentó, C.; Nieto, J. M. The Behavior of Trace Elements

670   during Schwertmannite Precipitation and Subsequent Transformation into Goethite and

671   Jarosite. *Geochim. Cosmochim. Acta* **2006**, *70* (16), 4130–4139.